PHYSICAL REVIEW A **86**, 012334 (2012)

Increasing the dimension in high-dimensional two-photon orbital angular momentum entanglement

J. Romero,[1,2] D. Giovannini,[1] S. Franke-Arnold,[1] S. M. Barnett,[2] and M. J. Padgett[1]
[1]*School of Physics and Astronomy, Scottish Universities Physics Alliance, University of Glasgow, Glasgow G12 8QQ, United Kingdom*
[2]*Department of Physics, Scottish Universities Physics Alliance, University of Strathclyde, Glasgow G4 ONG, United Kingdom*
(Received 20 March 2012; published 27 July 2012)

Any practical experiment utilizing the innate D-dimensional entanglement of the orbital angular momentum (OAM) of photons is subject to the generation capacity of the entangled photon source and the modal capacity of the detection system. We report an experimental spontaneous parametric-down-conversion system able to generate and detect tunable high-dimensional OAM entanglement. By tuning the phase matching, we demonstrate a factor of 2 increase on the half-width of the OAM-correlation spectrum, from 10 to 20. In terms of quantum mutual information capacity, this is an increase from 3.18 to 4.95 bits/photon. Furthermore, we measure correlations in the conjugate variable, angular position, and obtain concurrence values 0.96 and 0.90. The good entanglement measures in both OAM and angular position bases indicate bipartite, D-dimensional entanglement where D is tunable.

DOI: 10.1103/PhysRevA.86.012334 PACS number(s): 03.67.Bg, 03.65.Ud, 42.50.Ex, 42.50.Tx

I. INTRODUCTION

Much attention has been directed to the two-dimensional state space of photon polarization, which provides both a conceptually and experimentally accessible testbed [1–4]. An even more fertile testbed is D-dimensional two-photon entanglement, wherein each photon is a D-level qudit taking on any of D possible values. From a fundamental standpoint, higher-dimensional entanglement implies stronger violations of locality [5,6] and is especially useful in the study of mutually unbiased bases in higher dimensions [7]. More relevant to practical applications, higher-dimensional entanglement provides increased security and robustness [8–10] and a higher information capacity [9,11,12]. Entangled photon pairs typically come from the process of spontaneous parametric-down-conversion (SPDC) in a nonlinear crystal. High-dimensional entanglement between these photon pairs can broadly be classified into two groups. The first exploits the spectral [13] and temporal [14] degrees of freedom; an experimental system with at least 11 dimensions has been achieved for the latter [14]. The second exploits the spatial degrees of freedom such as transverse spatial profile [11] and transverse position and linear momentum [10,12,15]; an experimental system with a notable channel capacity of 7 bits/photon corresponding to roughly 128 dimensions has been reported for the latter. Most relevant to our work are studies exploiting the angular position and the orbital angular momentum, which relate to the modes with a spiral phase structure defined by the azimuthal index ℓ [16].

The entanglement of orbital angular momentum (OAM) in photons generated via SPDC is firmly established theoretically and experimentally [17,18]. The interest in OAM stems from its discrete and theoretically infinite-dimensional Hilbert space; ℓ could be any integer. Since the pioneering experiment of Mair *et al.* [18], OAM as well as its conjugate variable, angular position, has been steadily gaining ground as a mainstream variable in which to observe quantum correlations. Bell-type and Leggett inequalities have both been violated in two-dimensional OAM subspaces analogous to the experiments done previously for polarization [19,20]. The number of OAM modes is generally referred to as the spiral bandwidth [21]. The *generation* spiral bandwidth is the number of OAM modes that is produced by SPDC. The generation spiral spectrum of SPDC (i.e., the range of the D entangled OAM states and their respective weightings) has previously been calculated analytically from the coincidence fringe obtained from a clever angular equivalent of the Hong-Ou-Mandel interferometer using bucket detectors [22]. In contrast, the *measurement* spiral bandwidth is the number of OAM modes that can be measured. It depends on the generation spiral bandwidth and detection capability of the system.

Here we focus on the measurement spiral bandwidth, which dictates the number of usable OAM modes. Any projective measurement of OAM, wherein the OAM of the signal and idler photons are directly measured using a mode transformer (with a hologram or phase plate) and a single-mode fiber coupled to a photon detector, is inherently sensitive to the radial field distribution [22–24]. Measuring the OAM spectrum in this manner will inevitably result in a spiral bandwidth that is different from the generation bandwidth [22].

Pors *et al.* have calculated D from coincidence fringes as angular phase plate analyzers are rotated: D is the inverse of the area under the peak-normalized coincidence fringe [25]. Using this technique, a dimensionality of $D = 6$ has been measured for a SPDC system with a Schmidt number of 31. Another technique is to measure the OAM states of the signal and idler photons directly by forked diffraction holograms and build up a measurement spiral spectrum, as was done by Dada *et al.* in Ref. [6], where they have shown 11-dimensional OAM entanglement via generalized Bell inequalities. Using angular slits and forked diffraction holograms, Leach *et al.* successfully demonstrated the Einstein-Podolsky-Rosen paradox by measuring angular position and 15 different OAM states, although they did not obtain the dimensionality of the measured OAM entanglement [16]. In this work, we quantify the dimensionality of OAM entanglement via the quantum mutual information capacity, the information that is shared by the entangled photons. This is an especially meaningful quantity for quantum key distribution [12,26,27] and has not been measured for OAM previously. We measure 41 different OAM states and achieve an experimental quantum

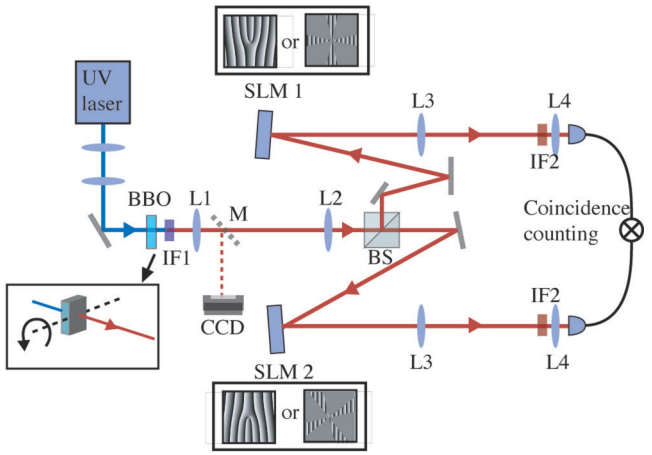

FIG. 1. (Color online) Experiment scheme. Photons from SPDC in a 5-mm-long BBO crystal are measured in the OAM or angular position basis by programming either a forked diffraction hologram or an angular four-slit pattern on the SLMs (inset). The SPDC phase matching is changed by tilting the BBO crystal about the axis shown (inset). The CCD camera accessible via the flip-up mirror M allows us to derive a phase-matching parameter according to Eq. (1).

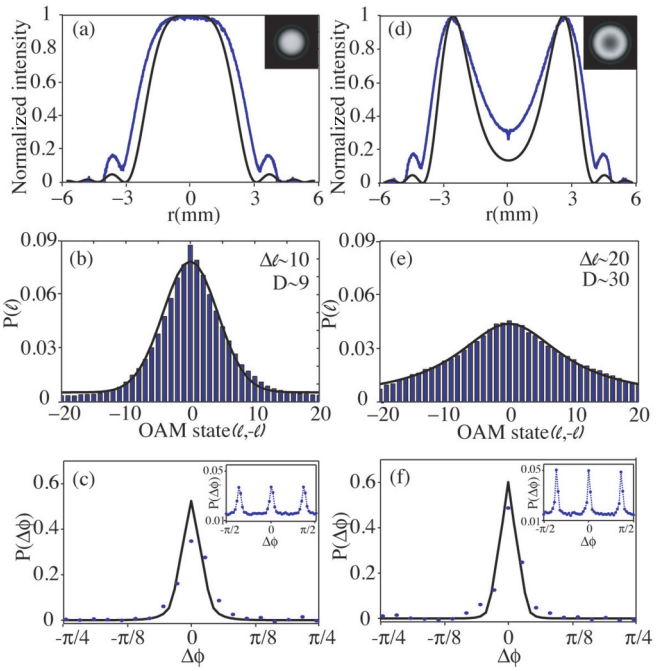

FIG. 2. (Color online) OAM and angular position measurements. (a) For collinear phase-matching, the far-field intensity profile (blue line) follows Eq. (1) (solid black line) with $\alpha = 0$. (b) The measured spiral spectrum has a half-width $\Delta\ell \approx 10$, with $D \approx 9$. (c) The central maximum (renormalised and background-subtracted) of our angular position correlation measurement when the signal and idler slits have a relative orientation of $\Delta\phi$, has a half-width of $\approx 12^\circ$. The inset shows the other maxima from the four-slit pattern. (d) For noncollinear phase-matching, $\alpha = -2.2$ in Eq. (1), the measurement spiral bandwidth is wider, with (e) $\Delta\ell \approx 20$, $D \approx 30$ and the angular position correlation is narrower, with (f) a half-width of $\approx 8^\circ$. Blue dots and bars are experiment results, solid black lines are fits that demonstrate consistency with a Fourier relation between OAM and angle.

mutual information capacity as high as 4.94 bits/photon corresponding to a dimensionality of ~ 30.

II. EXPERIMENT

To increase the number of measurable OAM modes, one can either optimize the detection system or widen the OAM spectrum of the generated two-photon state. These two are equally important, but optimizing detection is fruitless if the OAM states are not being generated in the first place. The detection geometry is more often fixed but can be designed optimally. The generation bandwidth can be modified by changing the characteristics of the pump beam [28,29] or by tuning the phase-matching conditions as shown previously by temperature tuning a periodically poled potassium titanyl phosphate crystal [22].

Our entangled photons are generated from a 5-mm-long β-barium-borate (BBO) crystal cut for type-1 collinear SPDC pumped by a collimated 355-nm pump beam (Fig. 1). The pump beam is blocked by a longpass filter (IF1) after passing through the crystal. The crystal is mounted on a rotation stage, which allows us to change the orientation of the crystal, consequently changing the phase matching from collinear to near collinear. The signal and idler fields are incident on the same beam splitter and imaged by lenses L1 ($f = 400$ mm) and L2 ($f = 200$ mm) to separate spatial light modulators (SLMs). A flip-up mirror (M) is used to direct the light to a CCD camera positioned at the focal plane of L1 to allow us to capture the far-field intensity of the down-converted fields [Figs. 2(a) and 2(d)]. The SLMs are imaged by lenses L3 ($f = 600$ mm) and L4 ($f = 3.2$ mm) onto the facets of single-mode fibers coupled to avalanche photodiodes (APDs) for single-photon detection. Bandpass filters (IF2) of width 10 nm and centered at 710 nm placed in front of the fibers ensure that we measure signal and idler photons near degeneracy. The outputs of the APDs are connected to a coincidence circuit and the coincidence rate is recorded as a function of the measurement states specified in the SLM.

Spontaneous parametric-down-conversion is the nonlinear interaction of three photons whose frequencies ω_j [j stands for the p (pump), s (signal), or i (idler) photon] are related as $\omega_p = \omega_s + \omega_i$. There is a range of wave vectors that will satisfy this energy conservation, and we can define an on-axis phase mismatch Δk_z from the z components of the wave vectors $\mathbf{k}_j$, $\Delta k_z = k_{p,z} - k_{s,z} - k_{i,z}$ [30]. The significance of phase matching has been realized previously in the seminal paper of Kleinman [30], in which he calls SPDC optical parametric noise. In any three-wave-mixing process, $2/\Delta k_z$ is the coherence length over which the three interacting fields remain in phase. In SPDC, Δk_z has implications for efficiency (SPDC is brightest when $\Delta k_z \sim 0$), but more importantly determines the spectral distribution of the down-converted photons [31,32]. Theoretical treatment of phase matching is complicated and several approximations have been made [29,33,34], but it is easy to do in practice by tuning either the temperature or angular orientation of the crystal [31]. In the case of our bulk crystal, changing the angular orientation changes the index of refraction for the pump beam and hence

Δk_z and the far-field intensity profile of the down-converted fields. The intensity profile I we obtain mirrors the sinc-phase-matching term in SPDC and is fitted with the function

$$I(r) = \mathrm{sinc}^2\left(\frac{ar^2}{f^2} + \alpha\right), \tag{1}$$

where r is radial coordinate in the focal plane of a lens with focal length f (L1), $\alpha = (|\mathbf{k}_p| - |\mathbf{k}_s| - |\mathbf{k}_i|)L/2$ is a phase-matching parameter that determines the opening angle of SPDC, and $a = (|\mathbf{k}_s| + |\mathbf{k}_i|)L/4n^2$, where n is the refractive index for the signal and idler wavelengths and L is the crystal length [35]. In the case where the transverse momentum of the photons is conserved, α is dominated by Δk_z; we take this as a measure of our on-axis phase mismatch and $\alpha = 0$ for the collinear case.

We measure both OAM and angle correlations for two different phase-matching conditions. To measure OAM, we encode forked diffraction gratings of topological charge ℓ_s on one SLM and ℓ_i on the other. These holograms transform the incoming field to a fundamental mode, which is the only mode that can be coupled to the fibers [18]. Since we are working in the collinear to near-collinear regime, OAM is conserved in our SPDC, hence we expect the OAM of the signal and idler photon to be anticorrelated, i.e., the coincidence count is high only when $\ell_s = -\ell_i$ [36]. Ideally, to measure correlations in angular position, we encode angular slits of width $\delta\phi$ centered at angle ϕ in both SLMs and rotate one with respect to the other, expecting high coincidence counts when the two slits are aligned [16]. Because the angle and OAM are Fourier related [37], a wide spiral bandwidth means a correspondingly narrow angular correlation that should be measured with a narrow angular slit. This presents a limitation in practice because a narrow angular slit means fewer counts, which are difficult to discern against the background. We solve this problem by using not one, but four narrow slits (7° wide, almost twice as narrow as what was used previously [16]) thereby enabling us to still measure tight angular correlations without sacrificing counts. With one four-slit pattern oriented at ϕ_s and another oriented at ϕ_i, we measure the coincidences as a function of $\Delta\phi = \phi_s - \phi_i$. As a result of having four slits, our angular position coincidence curves have more than one maximum [Figs. 2(c) and 2(f) insets] from which the width of the angular correlation can be derived.

Orbital angular momentum and angular position measurements for two different phase-matching conditions are shown in Fig. 2. We have judiciously subtracted the accidental counts $A = S \times I \times \Delta t$, where S and I are the single channel counts of the signal and idler arms, respectively, and $\Delta t = 10$ ns is our coincidence timing window. We define the measurement spiral bandwidth $\Delta\ell$ as the full width at half maximum of the measured spiral spectrum. For collinear phase matching $\alpha = 0$ in Eq. (1) [Fig. 2(a)], we find $\Delta\ell \approx 10$ [Fig. 2(b)] and the corresponding half-width of the central peak in the angular position coincidence curve is 12° [Fig. 2(c)]. With the addition of an on-axis phase mismatch $\alpha = -2.2$ in Eq. (1), the opening angle of the spot is slightly increased (to ≈1.1° from the propagation axis to the first minimum, compared to 0.9° for $\alpha = 0$). There is a central dip in the intensity distribution [Fig. 2(d)]; we find $\Delta\ell \approx 20$ [Fig. 2(e)]. The half-width of the corresponding angular position correlation is narrower, as expected from the Fourier relationship [37,38], and is 8°. The solid black lines in Figs. 2(b) and 2(e) are Lorentzian and are empirical fits to our data. Using these fits, we are able to calculate the expected angular correlation from the Fourier relation, with the added consideration that our angular masks have a finite slit width [solid line in Figs. 2(c) and 2(f)]. Angular position measurements are very sensitive to alignment, and we attribute the imperfect fits in Figs. 2(c) and 2(f) to this.

We focus on our OAM measurements and derive the mutual information H. This can be calculated from the probabilities $H = -\sum_{\ell_s} p(\ell_s)\log_2[p(\ell_s)] - \sum_{\ell_i} p(\ell_i)\log_2[p(\ell_i)] + \sum_{\ell_s,\ell_i} p(\ell_s,\ell_i)\log_2[p(\ell_s,\ell_i)]$, where $p(\ell_s,\ell_i)$ is the probability of measuring ℓ_s and ℓ_i, $p(\ell_s) = \sum_{\ell_i} p(\ell_s,\ell_i)$ is the probability of measuring ℓ_s, and $p(\ell_i) = \sum_{\ell_s} p(\ell_s,\ell_i)$ is the probability of measuring ℓ_i. For $\phi = 0$ the mutual information is 3.17 ± 0.60 bits/photon, corresponding to a dimensionality $D = 2^H \sim 9$. Adjusting the phase matching to $\phi = -2.2$ results in a mutual information of 4.94 ± 1.03 bits/photon, corresponding to $D \sim 30$, twice the measurement range of our previous results in Ref. [16]. We remark that apart from being detection limited, we have also defined our dimensionality stringently by calculating it from the mutual information. In this way we are sensitive to the level of noise and crosstalk even for measurements where $\ell_s \neq \ell_i$, which becomes more apparent with higher-valued OAM states. As such, we expect our dimensionality to be less than the Schmidt number K for our system. We have independently measured K for our system via sector phase plates and find these greater than our measured D. For $\phi = 0$ we obtain $K = 35 \pm 2$ and for $\phi = -2.2$ we obtain $K = 49 \pm 2$ [39]. The values of K can also be estimated from Ref. [33], which gives 35 for $\phi = 0$ and 43 for $\phi = -2.2$ with our experiment parameters. We also remark that K, being defined in terms of just probabilities, does not give any hint about the shape of the spiral spectrum. A full decomposition in terms of OAM modes has been treated elsewhere, albeit not for the noncollinear case [40,41]. The OAM spectrum, although not Lorentzian, is Lorentzian-like in shape and this has motivated us to use a Lorentzian fit [6,41]. Theoretical fits for our results and hence estimates for $\Delta\ell$ can only be obtained from a full model of our experiment, such as one based on the Klyshko backpropagation picture [42].

A simple geometrical argument can elucidate why the spiral spectrum widens as we tune the phase matching. This involves the concept of the optical étendue $E = A\Omega$, where A is the near-field beam area and Ω is the solid angle subtended by the beam in the far field [23,43]. In the treatment of noise in laser amplifiers, the étendue normalized with respect to the wavelength λ, E/λ^2, is the number of transverse modes that can be supported; E acts as a measure of the quantum states in a beam [43,44] and E is more often invoked in the discussion of light collection, but is equally applicable in the case of SPDC where light is instead being emitted. Regardless of the phase matching, A is the same in our experiment: The SLMs are in the near field of a particular plane in the crystal and minute changes to crystal orientation (typically 1/20 of a degree) do not change the image on the SLMs. However, this changes the far-field opening angle, Ω increases for $\alpha = -2.2$; hence the number of transverse (both azimuthal and radial) modes

emitted increases. In setting up a SPDC experiment, this has important practical implications: One should ensure that the detection étendue is greater than the generation étendue to maximize the overlap between the pump and detection modes. Using the Klyshko picture as a guide, where the detected signal (or idler) mode is backpropagated to the crystal, reflected off the crystal, and propagated to the other detector [42], the overlap is maximized by keeping all corresponding far-field solid angles and near-field beam diameters in the signal and idler arms the same. The reason we use two lenses to image the crystal onto the SLMs instead of one is to match the far-field angles in both arms and this gives us an effective detection system.

III. ENTANGLEMENT

Measuring the entanglement of D dimensions is not as straightforward as measuring the entanglement of two-dimensional systems. We can violate a Bell inequality for higher dimensions as implemented in Ref. [6], but this is difficult for $D \sim 30$ because the intensity mask reduces the count rates considerably. Instead, we employ the entanglement measure $E = \sum_{\ell_s,\ell_i} p(\ell_s,\ell_i) - p(\ell_s)p(\ell_i)$ proposed in Ref. [45], similar to the I-concurrence or Renyi-2 entropy apart from numerical factors. Here E is zero for separable states. For our results, we calculate values of 0.8101 ± 0.01 and 0.8097 ± 0.02 for $\phi = 0$ and -2.2, respectively, indicating that our two-photon OAM states are nonfactorable and therefore entangled. The presence of crosstalk in the higher OAM modes prevents us from getting a significantly higher entanglement measure for $\phi = -2.2$ as one might expect.

Furthermore, we exploit the Fourier relationship, or complementarity between OAM and angle [37,46], to characterize the entanglement in the angular position basis. When a photon passes through an angular aperture we can observe interference in the OAM distribution of the signal (or idler) field, the modulation of which depends on the spiral spectrum of the photons [47]. We can encode angular two-slit patterns on the SLMs [slits 1 and 2 in Fig. 3(a)] and measure the resulting OAM interference when SLM1 (idler) is set to measure $\ell_i = 0$ and the value of ℓ_s on SLM2 is scanned from $-\ell_{\max}$ to $\ell_{\max}$ ($\ell_{\max} = 20$ in our case). It has been shown that the visibility of the resulting interference pattern is the same as the concurrence (ranges from 0 to 1, 1 being the maximally entangled case) of the two-qubit density matrix written in the angular position basis [47,48]. We verify strong angular position correlation in Figs. 3(b) and 3(d), where we have measured the coincidences when we encode only one slit (of width 18°) on each SLM for both phase-matching conditions. As expected, we get appreciable coincidences only when we encode the same slit positions for both SLMs. Ideally the diagonals should be 0.5, but due to imperfect alignment we get small probabilities off the diagonal.

The interference of the two-slit patterns in Fig. 3(a) with their corresponding OAM values leads to a modulation in the coincidences that can be measured in the OAM basis. Figures 3(c) and 3(e) show the coincidences for $\alpha = 0$ [Fig. 3(b) inset] and $\alpha = -2.2$ [Fig. 3(d) inset]. The measured concurrence is 0.96 ± 0.07 for $\alpha = 0$ and 0.90 ± 0.12 for

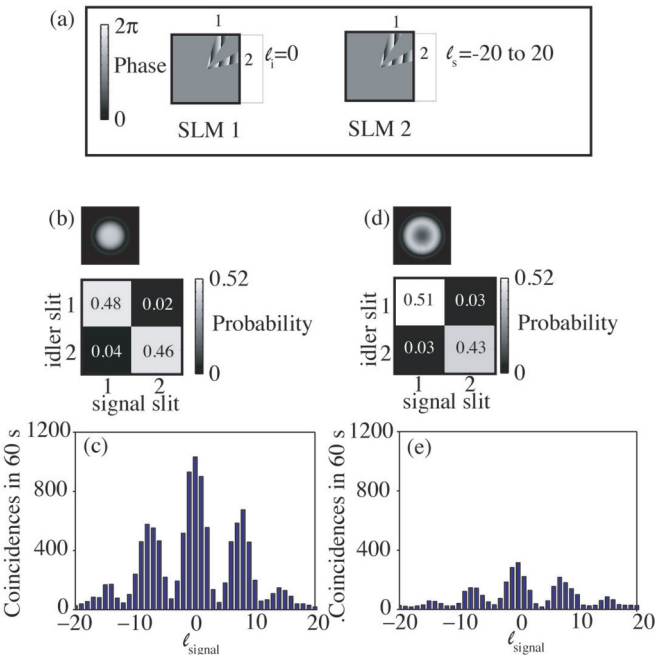

FIG. 3. (Color online) Concurrence measurements. (a) We encode two-slit patterns (width 18°, separated by 45°) in SLM1 and SLM2 with the corresponding OAM values shown. With only one slit in each SLM (1 or 2), we verify the strong angular position correlation. (b) For $\alpha = 0$, we get high coincidences only when both SLMs have slits with the same angular position. (c) The measured concurrence is 0.96. We show (d) a similar angular position correlation for $\alpha = -2.2$ and measure (e) a concurrence of 0.90.

$\alpha = -2.2$, demonstrating that we indeed have entangled angular qubit states for both phase-matching conditions. We remark that the decrease in the concurrence value is counterintuitive considering that the latter case corresponds to a greater number of OAM modes. This may be due to imperfect alignment, as measurements in the angular position basis are more sensitive to this. We also emphasize that the measurements made in Figs. 3(b) and 3(d) (strong angular position correlation) and Figs. 3(c) and 3(e) (interference in the OAM basis) can be produced simultaneously only by OAM-angular position entangled sources. The good entanglement measures in both OAM and angular position bases for both phase-matching conditions indicate genuine two-photon D-dimensional entanglement, where D is tunable.

IV. CONCLUSION

In conclusion, we have demonstrated a system where we can generate and detect high-dimensional two-photon entanglement. We have characterized the entanglement in terms of the mutual information shared by the entangled photon pairs. Minute changes to the angular orientation of a bulk BBO crystal (≈1/20 of a degree) widens the OAM measurement spiral spectrum and narrows the angular position correlation, as a consequence of phase matching in SPDC. We have designed our detection system guided by the concept of the optical étendue and we have achieved as much as 4.94 bits/photon, implying 30-dimensional OAM entanglement. We can obtain a relatively flat spectrum for a

few OAM modes, which could allow future protocols to forego entanglement concentration. We note that our measurements, although in a high-dimensional space, are still dichotomous, in contrast to a polarization beam splitter that sorts the two possible polarization states. However, a mode sorter that separates all of the D orthogonal OAM states has been recently developed [49]. Coupled with the generation and detection geometry that we have characterized in this work, this points to the possibility of new experiments such as detection loophole-free Bell test experiments [50], superdense coding [51,52] beating the linear optics threshold, and multivalued quantum walks [53] where a higher-dimensional space is desirable.

ACKNOWLEDGMENTS

This work was supported by EPSRC, DARPA InPho program, EU HIDEAS grant, Wolfson Foundation and the Royal Society. We thank Hamamatsu for the SLM loan and M. van Exter for useful discussions.

[1] A. Aspect, P. Grangier, and G. Roger, Phys. Rev. Lett. **47**, 460 (1981).
[2] N. Gisin, G. Ribordy, W. Tittel, and H. Zbinden, Rev. Mod. Phys. **74**, 145 (2002).
[3] R. Horodecki, P. Horodecki, M. Horodecki, and K. Horodecki, Rev. Mod. Phys. **81**, 865 (2009).
[4] M. Genovese, Phys. Rep. **413**, 319 (2005).
[5] D. Collins, N. Gisin, N. Linden, S. Massar, and S. Popescu, Phys. Rev. Lett. **88**, 040404 (2002).
[6] A. Dada, J. Leach, G. Buller, M. J. Padgett, and E. Andersson, Nat. Phys. **7**, 677 (2011).
[7] M. Wieśniak, T. Paterek, and A. Zeilinger, New J. Phys. **13**, 053047 (2011).
[8] H. Bechmann-Pasquinucci and A. Peres, Phys. Rev. Lett. **85**, 3313 (2000).
[9] H. Bechmann-Pasquinucci and W. Tittel, Phys. Rev. A **61**, 062308 (2000).
[10] L. Zhang, C. Silberhorn, and I. A. Walmsley, Phys. Rev. Lett. **100**, 110504 (2008).
[11] S. P. Walborn, D. S. Lemelle, M. P. Almeida, and P. H. Souto Ribeiro, Phys. Rev. Lett. **96**, 090501 (2006).
[12] P. B. Dixon, G. A. Howland, J. Schneeloch, and J. C. Howell, Phys. Rev. Lett **108**, 143603 (2012).
[13] M. Avenhaus, M. V. Chekhova, L. A. Krivitsky, G. Leuchs, and C. Silberhorn, Phys. Rev. A **79**, 043836 (2009).
[14] H. De Riedmatten, I. Marcikic, H. Zbinden, and N. Gisin, Quant. Inf. Comp. **2**, 425 (2002).
[15] J. C. Howell, R. S. Bennink, S. J. Bentley, and R. W. Boyd, Phys. Rev. Lett. **92**, 210403 (2004).
[16] J. Leach, B. Jack, J. Romero, A. Jha, A. Yao, S. Franke-Arnold, D. Ireland, R. Boyd, S. Barnett, and M. J. Padgett, Science **329**, 662 (2010).
[17] S. Franke-Arnold, S. M. Barnett, M. J. Padgett, and L. Allen, Phys. Rev. A **65**, 033823 (2002).
[18] A. Mair, A. Vaziri, G. Weihs, and A. Zeilinger, Nature (London) **412**, 313 (2001).
[19] J. Leach, B. Jack, J. Romero, M. Ritsch-Marte, R. W. Boyd, A. K. Jha, S. M. Barnett, S. Franke-Arnold, and M. J. Padgett, Opt. Express **17**, 8287 (2009).
[20] J. Romero, J. Leach, B. Jack, S. M. Barnett, M. J. Padgett, and S. Franke-Arnold, New J. Phys. **12**, 123007 (2010).
[21] J. P. Torres, A. Alexandrescu, and L. Torner, Phys. Rev. A **68**, 050301 (2003).
[22] H. Di Lorenzo Pires, H. C. B. Florijn, and M. P. van Exter, Phys. Rev. Lett. **104**, 020505 (2010).
[23] M. P. van Exter, A. Aiello, S. S. R. Oemrawsingh, G. Nienhuis, and J. P. Woerdman, Phys. Rev. A **74**, 012309 (2006).
[24] J. Romero, J. Leach, B. Jack, M. R. Dennis, S. Franke-Arnold, S. M. Barnett, and M. J. Padgett, Phys. Rev. Lett. **106**, 100407 (2011).
[25] J. B. Pors, S. S. R. Oemrawsingh, A. Aiello, M. P. van Exter, E. R. Eliel, G. W. 't Hooft, and J. P. Woerdman, Phys. Rev. Lett. **101**, 120502 (2008).
[26] T. Brougham and S. M. Barnett, Phys. Rev. A. **85**, 032322 (2012).
[27] J. Leach, E. Bolduc, D. J. Gauthier, and R. W. Boyd, Phys. Rev. A. **85**, 060304(R) (2012).
[28] J. P. Torres, Y. Deyanova, L. Torner, and G. Molina-Terriza, Phys. Rev. A **67**, 052313 (2003).
[29] F. M. Miatto, D. Giovannini, J. Romero, S. Franke-Arnold, S. M. Barnett, and M. J. Padgett, Eur. Phys. J. D **66**, 178 (2012).
[30] D. Kleinman, Phys. Rev. **174**, 1027 (1968).
[31] R. W. Boyd, *Nonlinear Optics* (Academic, New York, 2003).
[32] H. Vanherzeele and C. Chen, Appl. Opt. **27**, 2634 (1988).
[33] C. K. Law and J. H. Eberly, Phys. Rev. Lett. **92**, 127903 (2004).
[34] P. Kolenderski, W. Wasilewski, and K. Banaszek, Phys. Rev. A **80**, 013811 (2009).
[35] B. J. Pors, Ph.D. thesis, University of Leiden, 2010.
[36] C. I. Osorio, G. Molina-Terriza, and J. P. Torres, Phys. Rev. A **77**, 015810 (2008).
[37] A. K. Jha, B. Jack, E. Yao, J. Leach, R. W. Boyd, G. S. Buller, S. M. Barnett, S. Franke-Arnold, and M. J. Padgett, Phys. Rev. A **78**, 043810 (2008).
[38] B. Jack, P. Aursand, S. Franke-Arnold, D. G. Ireland, J. Leach, S. M. Barnett, and M. J. Padgett, J. Opt. **13**, 064017 (2011).
[39] D. Giovannini, F. Miatto, J. Romero, S. M. Barnett, J. P. Woerdman, and M. J. Padgett [New J. Phys. (to be published)].
[40] F. M. Miatto, A. M. Yao, and S. M. Barnett, Phys. Rev. A **83**, 033816 (2011).
[41] A. Yao, New J. Phys **13**, 053048 (2011).
[42] D. N. Klyshko, Sov. Phys. Usp. **31**, 74 (1988).
[43] T. Markvart, J. Opt. A **10**, 015008 (2008).
[44] A. Yariv, *Quantum Electronics* (Academic, New York, 1989).
[45] M. Cirone, Phys. Lett. A **339**, 269274 (2005).
[46] S. M. Barnett and D. T. Pegg, Phys. Rev. A **41**, 3427 (1990).
[47] A. K. Jha, J. Leach, B. Jack, S. Franke-Arnold, S. M. Barnett, R. W. Boyd, and M. J. Padgett, Phys. Rev. Lett. **104**, 010501 (2010).

[48] W. K. Wootters, Phys. Rev. Lett. **80**, 2245 (1998).
[49] G. C. G. Berkhout, M. P. J. Lavery, J. Courtial, M. W. Beijersbergen, and M. J. Padgett, Phys. Rev. Lett. **105**, 153601 (2010).
[50] T. Vértesi, S. Pironio, and N. Brunner, Phys. Rev. Lett. **104**, 060401 (2010).
[51] A. K. Pati, P. Parashar, and P. Agrawal, Phys. Rev. A **72**, 012329 (2005).
[52] J. Barreiro, T. Wei, and P. Kwiat, Nat. Phys. **4**, 282 (2008).
[53] A. Schreiber, K. N. Cassemiro, V. Potoček, A. Gábris, P. J. Mosley, E. Andersson, I. Jex, and C. Silberhorn, Phys. Rev. Lett. **104**, 050502 (2010).